

U-SHAPED OUTFLOW IN THE LYNDS 1221 DARK CLOUD: AN EXAMPLE OF INTERACTION OF OUTFLOWS WITH AMBIENT MOLECULAR CLOUDS

TOMOFUMI UMEMOTO,^{1,2,3} NAOMI HIRANO,¹ OSAMU KAMEYA,¹ YASUO FUKUI,² NARIO KUNO,³ AND KEIYA TAKAKUBO³

Received 1990 June 19; accepted 1991 February 26

ABSTRACT

We report molecular line observations of the dark cloud L1221 in the $J = 1-0$ transitions of CO, ^{13}CO , C^{18}O , HCO^+ , HCN, and CS with angular resolutions of $17''-2.7''$. We have discovered a bipolar CO outflow associated with IRAS 22266+6845. The outflow shows a remarkably bent *U-shaped* structure. The present observations show rather clear evidence for interaction of the outflow with the ambient molecular gas; the ambient gas shows density depression and velocity shift just toward the blue lobe of the outflow. This fact indicates the acceleration and exclusion of the ambient gas by the outflow. The outflow changes its direction in accordance with the dense gas ridge. However, this ridge alone is not likely to be responsible for the outflow morphology, indicating that an external agency to form the outflow morphology is required.

Subject headings: interstellar: molecules — nebulae: individual (Lynds 1221) — nebulae: internal motions — stars: formation

1. INTRODUCTION

Molecular outflows are frequently associated with young stellar objects over an enormous range of luminosity (e.g., Lada 1985). The outflows have vast mechanical energies and momenta, suggesting that they may have a significant influence on the dynamics and evolution of giant molecular clouds via interaction (Margulis & Lada 1986; Fukui et al. 1986; Margulis, Lada, & Snell 1988). However, it is not well understood as yet how the outflow interacts with the ambient material, because the structure and kinematics of the material surrounding the outflow have been paid little attention. We have to investigate not only the structure and velocity field of the outflow but also those of the parent cloud. Recent millimeter-wave and infrared observations have revealed that numbers of outflows are frequently associated with low-luminosity infrared sources in dark clouds (e.g., Beichman et al. 1986; Myers et al. 1988; Fukui 1989). The detailed studies of the ambient gas around the outflow have been performed on several dark clouds, and it is suggested that outflows could have a profound influence on structure and dynamics of clouds (e.g., Goldsmith, Langer, & Wilson 1986; Myers et al. 1988; Mathieu et al. 1988). However, the spatial resolutions of the previous studies are not enough for throwing light on interacting regions. In addition, they are mainly concentrated on the dense cores or disks (e.g., probed by NH_3) surrounding young stellar objects, but pay little attention to relatively low-density gas (e.g., probed by ^{13}CO). In order to elucidate the interaction process, it is important to make high-resolution mapping for the ambient gas surrounding the outflow by using molecular lines which probe various density regions.

From an extensive survey of dark clouds with the 4 m radio telescope of Nagoya University, we have discovered a bipolar CO outflow associated with IRAS 22266+6845 (*IRAS Point Source Catalog* 1988) in L1221 (see the catalog of outflows compiled by Fukui 1989). This outflow was found indepen-

dently by Haikala & Dietrich (1989) with the University of Cologne 3 m telescope. In order to make clear the interaction of the outflow with its ambient gas, we have made high-resolution mappings in various molecular lines for the L1221 dark cloud using the 45 m telescope at Nobeyama Radio Observatory.

On the POSS plate, L1221 is an isolated object, and is easily identified. This cloud has a sharp boundary toward the south. It is located at $l = 110^\circ.7$ and $b = 9^\circ.6$, and has an opacity class 5 with about $10'$ diameter in the Lynds (1962) Dark Nebulae Catalogue. The POSS red plate shows faint nebulosities in the central part of the cloud (designated as GN 22.26.01 in the Atlas of Galactic Nebulae [Neckel & Vehrenberg 1987]), and they are associated with IRAS 22266+6845. This *IRAS* source has a total luminosity of $2.7 L_\odot$, when we assume the distance to L1221 to be 200 pc, the same distance as the neighboring cloud L1235 (Snell 1981).

We have selected the small isolated dark cloud L1221 as one of the suitable objects to study the interaction of the outflow with the ambient gas. Because molecular line widths in the ambient gas of dark clouds are generally small, it is easy to detect a disturbance of velocity field caused by interaction of the outflow. In addition, a small dark cloud could be violently disturbed by a molecular outflow because the size and energy of an outflow become comparable to those of a small cloud (Moriarty-Schieven & Snell 1988). In fact, molecular line width in the L1221 region is relatively small ($\sim 1 \text{ km s}^{-1}$), and the outflow has a size comparable to that of the cloud.

In this paper we will describe the discovery of the CO outflow in the L1221 dark cloud, and show both morphological and dynamical evidence for interaction of the outflow with the ambient gas. Observational methods are described in § 2. Results and physical parameters for the outflow and the molecular cloud are presented in § 3. In § 4 we discuss the dynamical interaction of the outflow with the ambient cloud, and present possible interpretations of the outflow morphology.

2. OBSERVATIONS

We used the 4 m millimeter-wave telescope at Nagoya University (Kawabata et al. 1985) to obtain the CO distribution in

¹ Nobeyama Radio Observatory, National Astronomical Observatory, Nobeyama, Minamisaku, Nagano 384-13, Japan

² Department of Astrophysics, Nagoya University, Chikusa-ku, Nagoya 464-01, Japan

³ Astronomical Institute, Tohoku University, Sendai 980, Japan

the L1221 dark cloud. The half-power beamwidth of the telescope was 2.7, with a main-beam efficiency of 0.7 at 110 GHz. High-velocity CO $J = 1-0$ emission in the region around IRAS 22266 + 6845 was observed in 1986 November and December in the position-switching mode. The receiver front end was a 15 K cooled Schottky mixer receiver, which provided a receiver noise temperature of 200 K (double sideband [DSB]). Spectra were taken with an acousto-optical spectrometer with frequency resolution and bandwidth of 40 kHz and 44 MHz, respectively. The outflow was fully mapped with a grid spacing of 2' in the CO line (Fig. 1).

Observations of the quiescent cloud in ^{13}CO and C^{18}O were carried out in 1989 December in the frequency-switching mode. The receiver front end was a 4 K cooled Nb SIS mixer with a receiver temperature of 70–80 K (DSB) and a typical system temperature of 250 K (single sideband [SSB]). The back end was an acousto-optical spectrometer having a frequency resolution of 48 kHz. The ^{13}CO emission was mapped over a region of about $20' \times 46'$ at a grid spacing of 2' (Fig. 4). We mapped the central core region of $16' \times 16'$ in C^{18}O on a 2' grid (Fig. 5). To express observed positions, we shall use offsets ($\Delta\text{R.A.}$, $\Delta\text{decl.}$) from IRAS 22266 + 6845, which is located at $\text{R.A.}(1950) = 22^{\text{h}}26^{\text{m}}37^{\text{s}}.2$, $\text{decl.}(1950) = 68^{\circ}45'52''$.

Using the 45 m telescope at the Nobeyama Radio Observatory⁴ (NRO), we observed the $J = 1-0$ lines of CO (115.271 GHz), ^{13}CO (110.201 GHz), HCO^+ (89.189 GHz), HCN (88.632 GHz), and CS (48.991 GHz) in four days in 1988 April. The telescope had a beam size of 17" with a main-beam efficiency of 0.45 at 110–115 GHz. The pointing accuracy was better than 5" as determined by observing the SiO maser source T Cep at 43 GHz or at 86 GHz every 2 hours. We employed two cooled Schottky mixer receivers. One provided SSB system temperatures of 650–1100 K at 110–115 GHz, and the other provided 500 K at 89 GHz. For CS observations, we used an SIS mixer receiver with a system temperature of 450 K at 49 GHz. The telescope beam was divided into two orthogonal polarizations with a polarization splitter, and then fed into the two receivers. We have made observations with three combinations of (CO and CS), (CO, HCO^+ , and HCN), and (^{13}CO and CS); here the parentheses enclose simultaneous observations. Spectra were taken with acousto-optical spectrometers having an effective frequency resolution of 37 kHz (a

channel interval of 20 kHz) and a bandwidth of 40 MHz. We used a "multi-ON-OFF" switching mode; nine ON-positions and three OFF-positions were observed sequentially for each scan. The inner region around the IRAS source was mapped at a grid spacing of 15", while the outer region was mapped at a grid spacing of 30".

We corrected the spectral line intensity for the atmospheric extinction using the chopper-wheel method (Kutner & Ulich 1981). The absolute intensity scale of the 4 m telescope data was established by referring to S140, whose CO and ^{13}CO peak radiation temperatures T_R^* were assumed to be 20 and 9 K, respectively. As for the C^{18}O line, we adopted the same factor as that for the ^{13}CO line. The absolute intensity scale of the 45 m telescope CO data was obtained by assuming that the CO peak intensity of the L1221 quiescent cloud is the same as the 4 m telescope data. This procedure would be valid because the CO peak intensity of the quiescent cloud is fairly constant over a scale of $\sim 5'$. We assumed that the absolute intensity scale of ^{13}CO was the same as the scale of CO. The absolute intensities of HCO^+ , HCN, and CS were corrected for the main-beam efficiency. Observational parameters using the 4 m and 45 m telescopes are summarized in Table 1.

3. RESULTS

3.1. CO Molecular Outflow

We have discovered high-velocity CO emission toward IRAS 22266 + 6845 using the 4 m telescope. The spatial distribution of the blue- and redshifted wing emission is shown in Figure 1. The high-velocity gas shows a clear bipolar pattern directed in the northeast-southwest direction with a size of 0.5 pc \times 0.3 pc. The center of the wing distribution is located near IRAS 22266 + 6845, suggesting that this source is the driving source of the outflow. This outflow was found independently by Haikala & Dietrich (1989) using the University of Cologne 3 m telescope, whose half-power beamwidth is 3.9. The blue and red components on their map are more extended than those on our map. This can be explained in terms of the difference of angular resolutions between two telescopes and the difference in the velocity integration range.

We used the NRO 45 m telescope to investigate the detailed structure and morphology of the outflow. The map of the CO wings obtained with the 45 m telescope (Fig. 2) shows details not seen on that obtained with the 4 m telescope. The most prominent feature of the CO outflow is a U-shaped structure opened to the northwest. Here we view the morphology of the lobes of the outflow. First, near the IRAS source [the offset

⁴ Nobeyama Radio Observatory is a branch of the National Astronomical Observatory, an interuniversity research institute operated by the Ministry of Education, Science, and Culture, Japan.

TABLE 1
MOLECULAR OBSERVATIONS TOWARD L1221

Molecular Transition	Beam Size	η_B^a	Velocity Resolution (km s^{-1})	Position	$T_R^*(\text{peak})$ (K)	rms Noise (K)	$V_{\text{LSR}}(\text{peak})$ (km s^{-1})	$\Delta V(\text{FWHM})$ (km s^{-1})
4 m telescope:								
CO $J = 1-0$	2.7	0.7	0.10	(0", 0")	8.8	0.4	-4.2	2.2
^{13}CO $J = 1-0$	2.7	0.7	0.13	(0", 0")	4.9	0.3	-4.2	1.4
C^{18}O $J = 1-0$	2.7	0.7	0.13	(0", 0")	1.2	0.1	-4.2	1.0
45 m telescope:								
CO $J = 1-0$	17"	0.45	0.10	(45" - 30") ^b	10.2	0.7	-4.4	3.0
^{13}CO $J = 1-0$	18"	0.45	0.10	(45", -30") ^b	8.2	0.8	-4.3	1.4
HCO^+ $J = 1-0$	21"	0.65	0.12	(45", -30") ^b	6.3	0.5	-4.4	1.0
HCN $J = 1-0$	21"	0.65	0.12	(45", -30") ^b	1.7	0.5	-4.4	0.8
CS $J = 1-0$	36"	0.85	0.23	(45", -30") ^b	2.7	0.3	-4.3	1.1

^a Main-beam efficiency.

^b Intensity peak position.

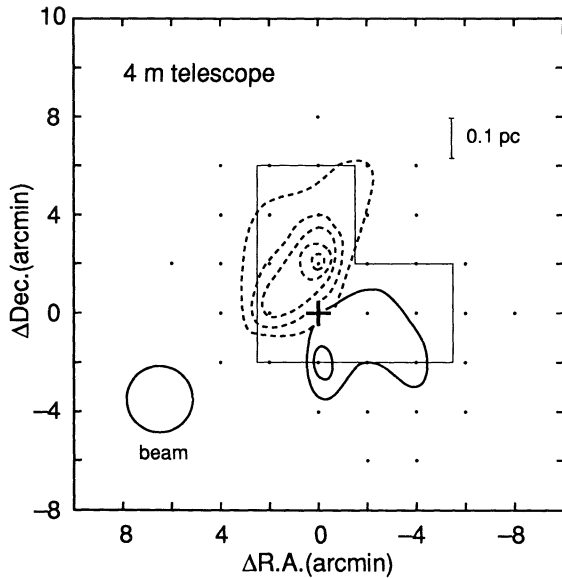


FIG. 1.—Contour map of the high-velocity CO emission in L1221 obtained with the 4 m telescope. The velocity integration range for the blue wing (*dashed line*) is from -8.5 to -6.5 km s^{-1} , and that for the red wing (*solid line*) is from -2.5 to -0.5 km s^{-1} . The cross indicates the position of IRAS 22266 + 6845, at R.A.(1950) = $22^{\text{h}}26^{\text{m}}37^{\text{s}}.2$ and decl.(1950) = $68^{\circ}45'52''$. Position offsets are measured from IRAS 22266 + 6845. Dots denote the points observed with the 4 m telescope. The observed area with the 45 m telescope is indicated by a thin-lined box.

position of (0'0, 0'0) to (1'5, 1'0)], the blue lobe is well collimated and most intense. It is elongated toward the northeast; its position angle is $\sim 50^{\circ}$. This direction is parallel to the sharp southern edge of the quiescent cloud (see Fig. 4 or Fig. 5). Next, going away from the *IRAS* source [a range from (1'5, 1'0) to (1'5, 4'0)], the blue lobe changes the direction to the north. In this range, the blue lobe becomes less intense but broader.

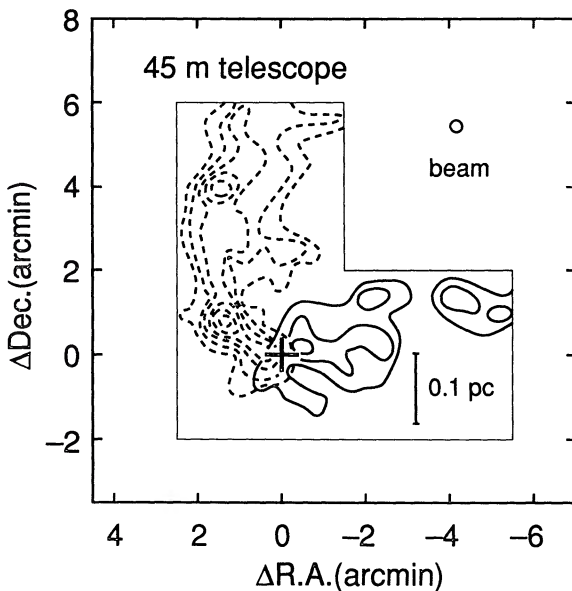


FIG. 2.—High-resolution map of the high-velocity CO emission taken with the 45 m telescope. The integration ranges of velocities are the same as those in Fig. 1. Contours are very 1.25 K km s^{-1} , with the lowest contour at 2.5 K km s^{-1} . The area mapped at $15''$ – $30''$ grid spacing interval is indicated by a thin-lined box.

Finally, in the northern part from (1'5, 4'0), the blue lobe changes its direction again; its position angle is $\sim 150^{\circ}$. On the other hand, the red lobe is elongated toward the west and does not greatly change its position angle. We find isolated redshifted emission to the west side, around the offset position of $(-4.5, 1'0)$, which reaches the edge of the molecular cloud (see Fig. 5). We suppose that this component is a part of the red lobe of the outflow associated with IRAS 22266 + 6845.

Figure 3 shows a typical example of CO and ^{13}CO spectra averaged over six channels (~ 0.3 km s^{-1} velocity resolution). A full velocity extent of the CO wing is ~ 14 km s^{-1} at a 1σ noise level of 0.1 K at (0'', 0''), that is, the maximum observed velocity of the outflow, V_{max} , becomes 7 km s^{-1} . The extent of the blue- and redshifted emission, defined as maximum separation from the *IRAS* point source at the half-intensity level, is ~ 0.36 pc each. By using this extent and V_{max} , we have estimated the dynamical time scale to be $\sim 5 \times 10^4$ yr. This means that the outflow in L1221 is not so young (see, e.g., Lada 1985; Levreault 1988; Fukui 1989).

We estimated the physical parameters of the outflow, following Iwata, Fukui, & Ogawa (1988). Here we used only the data taken with the 45 m telescope for the calculations. At the positions where the intense CO wings are seen, the ^{13}CO line

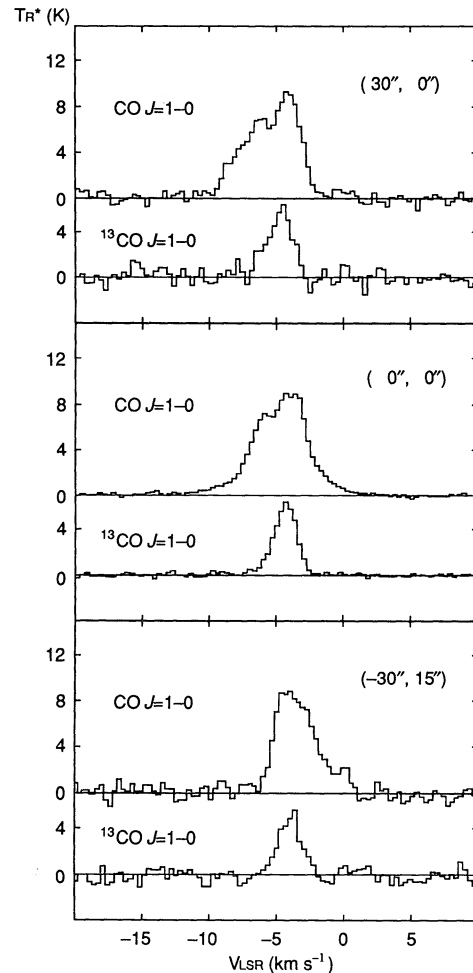


FIG. 3.—CO and ^{13}CO profiles obtained with the 45 m telescope at $(\Delta\text{R.A.}, \Delta\text{decl.}) = (30'', 0'')$, $(0'', 0'')$, and $(-30'', 15'')$, where the blue and red wing are prominent. The offset center is the position of the *IRAS* point source. These profiles are averaged over six channels (~ 0.3 km s^{-1} velocity resolution).

spectra also show wings. We estimated the mass of the outflow using this ^{13}CO wing assuming local thermodynamical equilibrium (LTE). The excitation temperature of the outflow gas is assumed to be 12 K, which is the same as that of the quiescent cloud gas (see § 3.2). The ^{13}CO column densities of the outflow for the blue and the red wings, where the ^{13}CO wing is seen, were integrated from -7.0 to -5.5 km s^{-1} and from -3.0 to -2.5 km s^{-1} , respectively. The mass of the outflow was calculated by integrating the H_2 column density determined on the assumption that the abundance ratio of H_2 to ^{13}CO was 5.0×10^5 (Dickman 1978). The momentum and kinetic energy were calculated as two extreme cases. For case I we calculate those values assuming that the outflow material is moving at the velocity which we have just observed. For case II we calculate them assuming that all material is moving at the maximum observed velocity, V_{max} , in CO. Estimated physical parameters of L1221 outflow are listed in Table 2. We assumed that the actual momentum and kinetic energy of the outflow lie between the values of the two cases. If the outflow has an inclination nearly perpendicular to the line of sight, even V_{max} may underestimate the actual outflow velocity (e.g., Snell & Schloerb 1985; Hirano et al. 1988). Since we cannot obtain any reasonable guess at the inclination of the outflow, here we shall adopt the momentum, kinetic energy, and mechanical luminosity, by geometrical averaging of the above two cases. The total mass, momentum, energy, and mechanical luminosity of this outflow are $1.3 M_{\odot}$, $4.4 M_{\odot} \text{ km s}^{-1}$, 1.5×10^{44} ergs, and $0.026 L_{\odot}$, respectively.

These values are comparable to the geometrical averages of the lower and upper limits of molecular outflows, e.g., B335, L1455, and L723 (Goldsmith et al. 1984), which are associated with the low-luminosity infrared sources in dark clouds. On the other hand, these values are greater than those of outflows discovered in dark clouds by Heyer et al. (1987) and Meyers et al. (1988). Hence, the outflow in L1221 is a relatively energetic one in dark clouds. Another characteristic of this outflow is the difference in physical parameters between the blue- and redshifted components. The mass, momentum, and energy for the blueshifted component are factors of 3–5 larger than those of the redshifted one.

3.2. Quiescent Molecular Cloud and Dense Core

We show the contour map of the ^{13}CO peak radiation temperature superposed on the POSS red print in Figure 4. The 1.0 K contour extends over the region of $\sim 16' \times 40'$ (~ 1.0 pc \times 2.4 pc), and the ^{13}CO distribution is closely coincident

with that of the visual extinction on the POSS print. The ^{13}CO intensity drops sharply in the southeast boundary of the cloud, while it extends to the northwest. The dense core region is located in the southeast corner of the map at the central (0', 0') position, which corresponds to the position of IRAS 22266 + 6845, and we will call this region the " ^{13}CO core." The half-intensity level of the ^{13}CO core has a size of $9.5' \times 10.5'$, or 0.57 pc \times 0.63 pc. Both excitation and gas kinetic temperatures were taken to be 12 K, which was calculated from the CO peak intensity assuming that this line is optically thick. This would not change so much over the ^{13}CO core region because the spatial distribution of the CO peak intensity is fairly uniform. The ^{13}CO optical depth was estimated to be about 0.8 at the IRAS source. Then the LTE column density of molecular hydrogen was estimated as $N(\text{H}_2) = 4.9 \times 10^{21} \text{ cm}^{-2}$ at the IRAS source. The mass and average density of the ^{13}CO core were calculated to be $30 M_{\odot}$ and $3.9 \times 10^3 \text{ cm}^{-3}$, if the core is a sphere with a mean radius of 0.30 pc. We derived the quiescent cloud mass within the lowest contour level in Figure 4 to be $45 M_{\odot}$.

The higher column density region of the cloud has been mapped in the C^{18}O line (Fig. 5). The distribution of the integrated intensity of the C^{18}O line extends toward the north and the northwest directions. The C^{18}O core has a size of $5.4' \times 6.3'$ (0.32 pc \times 0.38 pc), and peaks near IRAS 22266 + 6845. We derived physical parameters in the C^{18}O core by comparing ^{13}CO and C^{18}O lines. The ^{13}CO to C^{18}O abundance ratio was taken here to be a terrestrial value of 5.5. The optical depth of the C^{18}O was estimated to be ~ 0.13 at the IRAS source. Adopting the excitation temperature of 12 K, we obtained the column density of molecular hydrogen, $N(\text{H}_2) = 3.1 \times 10^{21} \text{ cm}^{-2}$. We derived the mass of the C^{18}O core to be $6 M_{\odot}$ and the mean density to be $5.0 \times 10^3 \text{ cm}^{-3}$, assuming a spherical core with a mean radius of 0.17 pc.

The C^{18}O line is useful to probe high column density regions but not always to probe high volume density regions. We used the lines of CS $J = 1-0$, $\text{HCO}^+ J = 1-0$, and HCN $J = 1-0$ in order to probe the denser gas [$n(\text{H}_2) > 10^4 \text{ cm}^{-3}$] surrounding the infrared source. Contour maps of total integrated intensity in CS, HCO^+ , and HCN lines are shown in Figures 6a, 6b, and 6c. The CS distribution shows a *V-shaped* structure elongated along the northwest-southeast and northwest-southwest. The angular size of the CS core at half-intensity level is $2.2' \times 2.0'$, corresponding to 0.13 pc \times 0.12 pc. The emission peak of the CS core is located at ($45''$, $-30''$), 0.06 pc distant from IRAS 22266 + 6845, while the emission shows no significant enhance-

TABLE 2
PHYSICAL PARAMETERS OF THE L1221 OUTFLOW

COMPONENT	V_{max}^a (km s^{-1})	SIZE ^b (pc)	DYNAMICAL TIME SCALE ^c (yr)	MASS ^d (M_{\odot})	MOMENTUM ^e ($M_{\odot} \text{ km s}^{-1}$)		ENERGY ^e (10^{44} ergs)		MECHANICAL LUMINOSITY ^e (L_{\odot})	
					Case I	Case II	Case I	Case II	Case I	Case II
Blue	7.6	0.36	4.6×10^4	1.0	1.7	7.6	0.27	5.8	0.0048	0.10
Red	6.5	0.36	5.4×10^4	0.3	0.3	2.0	0.06	1.3	0.0008	0.02
Total	14.1	1.3	2.0	9.6	0.33	7.1	0.0056	0.12

^a Maximum velocity shift of CO $J = 1-0$ emission from $V_{\text{LSR}} = -4.2 \text{ km s}^{-1}$ at 1σ level.

^b Size was defined as maximum separation from the IRAS point source to a point at half-infinity level.

^c Dynamical time scale was calculated by dividing the radius by V_{max} .

^d Determined for the velocity ranges -7.0 to -5.5 km s^{-1} and -3.0 to -2.5 km s^{-1} , where $^{13}\text{CO } J = 1-0$ wings are seen.

^e For case I we calculate those values assuming that the outflow material is moving at the velocity which we have just observed. For case II we calculate them assuming that all material is moving at the maximum observed velocity, V_{max} (Iwata, Fukui, & Ogawa 1988).

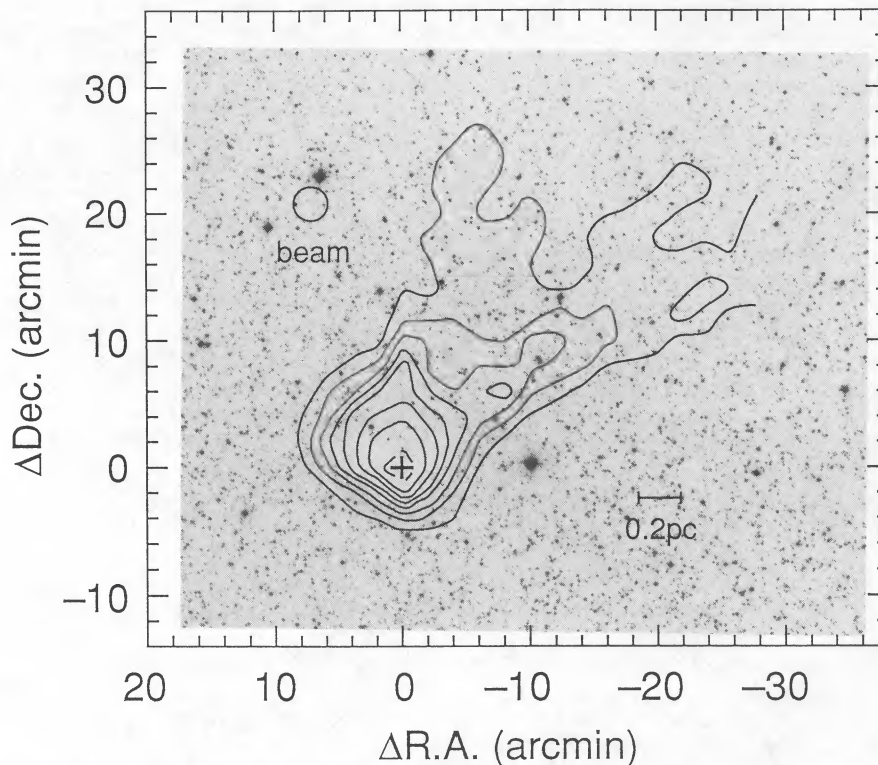


FIG. 4.—Contour map of the peak ^{13}CO radiation temperature in the region of L1221 taken with the 4 m telescope. This map is superposed on a copy of the POSS red plate. IRAS 22266 + 6845 is indicated by a cross. Contours are every 1.0 K, with the lowest contour at 1.0 K.

ment at the *IRAS* position. The distribution of HCO^+ emission shows an elongated structure mainly along the northwest-southeast direction with an extent of 2.2×2.0 at half intensity level. The northeast-southwest elongation,

however, is not clear. The strong emission peak is located also at $(45'', -30'')$, and the weak one corresponds to the *IRAS* source position $(0'', 0'')$. The extent of the HCN emission is about half of those in CS or HCO^+ . We note that it shows clear evidence for two separate peaks; one is centered on the *IRAS* source, and the other is at the intensity peaks of CS and HCO^+ emission.

We estimate the mass of the dense core by using the CS data. CS has a relatively high dipole moment ($= 1.96$ debye), and the critical density of exciting the CS $J = 1-0$ line is $1 \times 10^5 \text{ cm}^{-3}$. For the higher optical depth, $\tau \gg 1$, we can observe material whose density is smaller than the critical density by a factor of τ . In fact, the optical depth of the CS line in dark clouds is higher than unity; it is estimated to be 2–3 (e.g., Kaifu et al. 1984; Snell, Langer, & Frerking 1982). We assume that the mean density of CS emitting gas is $4 \times 10^4 \text{ cm}^{-3}$. Then the mass of the CS core with 0.06 pc radius is estimated to be $\sim 2 M_{\odot}$, which is one-third of the mass of the C^{18}O core. Physical parameters of the dense cores are listed in Table 3.

3.3. Morphological Comparison of the Ambient Cloud with the CO Outflow

We will compare the distribution of the ambient gas with that of the CO outflow in this subsection. First, we discuss the morphological coincidence of the C^{18}O core and the CO outflow. The distribution of the C^{18}O emission obtained by the 4 m telescope shows elongated structure toward the north and the northwest directions. The blue lobe of the CO outflow is aligned along the north elongation (see Fig. 5). This elongation of the C^{18}O core roughly delineates the eastern limb of the blue lobe, suggesting that there is a considerable amount of material on the southeast and east sides of the blue lobe. It

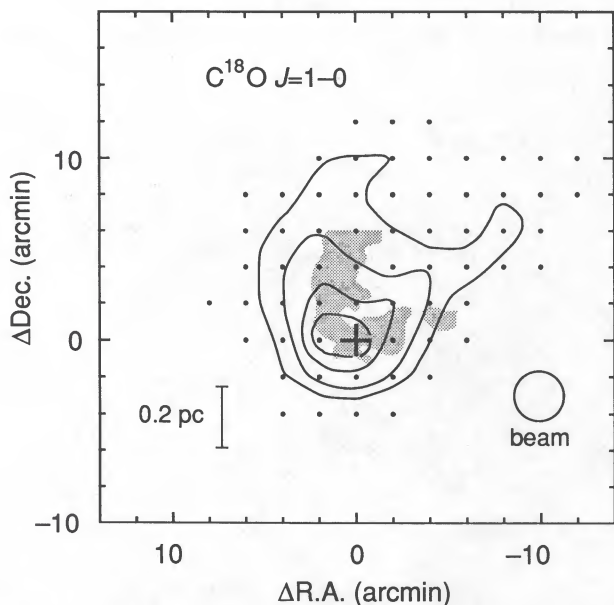


FIG. 5.—Contour map of the C^{18}O integrated intensity over the velocity range from -5.5 to -3.0 km s^{-1} . The contours are every 0.2 K km s^{-1} , with the lowest contour of 0.2 K km s^{-1} . The cross indicates IRAS 22266 + 6945. The stippled region denotes the area of the high-velocity CO emission detected above the 2.5 K km s^{-1} level with the 45 m telescope as shown in Fig. 2.

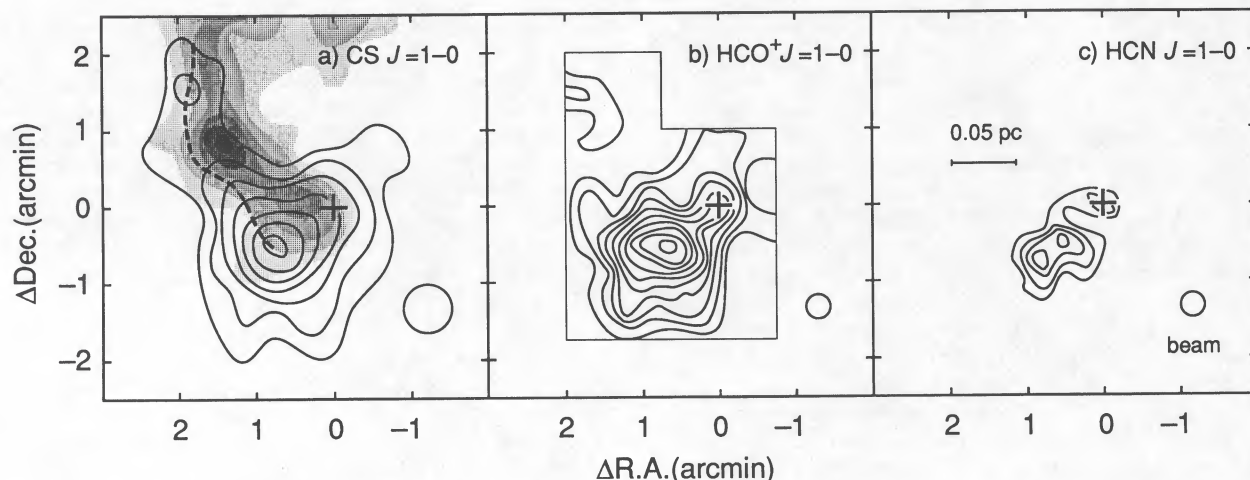


FIG. 6.—(a) Contour map of the integrated intensity of CS $J = 1-0$ emission in L1221 taken with the NRO 45 m telescope (*thin solid line*) superposed on the map of the CO blue lobe (*gray scale*). The line intensity is integrated in the velocity range from -6 to -3 km s^{-1} for all three panels. Contours are drawn every 0.3 K km s^{-1} , with the lowest contours at 0.9 K km s^{-1} . The mapped area is the same as in Fig. 2. The cross indicates IRAS 22266+6845. The ridge of the CS emission delineating the eastern limb of the CO blue lobe is denoted by a dashed line. (b) Contour map of the integrated intensity of $\text{HCO}^+ J = 1-0$ emission. Contours are drawn every 0.6 K km s^{-1} , with the lowest contours at 1.8 K km s^{-1} . The mapped area with $15''$ grid spacing interval is indicated by a line surrounding the contours. (c) Contour map of the integrated intensity of the HCN $J = 1-0$ emission. Contours are drawn every 0.3 K km s^{-1} , with the lowest contours at 0.9 K km s^{-1} . The mapped area is the same as that in (b).

seems that this material regulates the direction of the CO outflow.

Next, we discuss the high-density gas around the CO outflow. We have shown that the CS core has a *V-shaped* structure. The northwest-southeast elongation is perpendicular to the axis of the CO blue lobe in this region. We find also a weak ridge of the CS emission directed toward the northeast direction from its peak, which is parallel to the blue lobe. This ridge (*thick dashed line* in Fig. 6a) delineates the southeast limb of the blue lobe, which has an intensity gradient there. This indicates that high-density gas exists along the southeastern side of the CO outflow. Note that the CO blue lobe changes its direction from northeast to north along the dense gas ridge.

Finally, we discuss the ^{13}CO distribution with data of high angular resolution in the cloud central region. In Figure 7 we show the spatial distribution of the ^{13}CO integrated intensity around the IRAS source. The velocity integration is chosen to eliminate the contribution from ^{13}CO wings. The ^{13}CO distribution shows that the two peaks lie on both sides of the IRAS source with an angular separation of $1''.25$ ($=0.075$ pc) along the northwest-southeast direction, which is the same

direction as the elongation of the CS and the HCO^+ core. This direction is perpendicular to the axis of the CO blue lobe in this region.

It is remarkable that the ^{13}CO emission is relatively weak toward the blue lobe of the CO outflow. The spatial distribution of the ^{13}CO emission shows the "bay" structure open to the northeast and an anticorrelation with the CO blue lobe. The local minimum of ^{13}CO emission at $(60'', 30'')$ is located just at the CO blue lobe. Within the "bay," the cloud gas seems

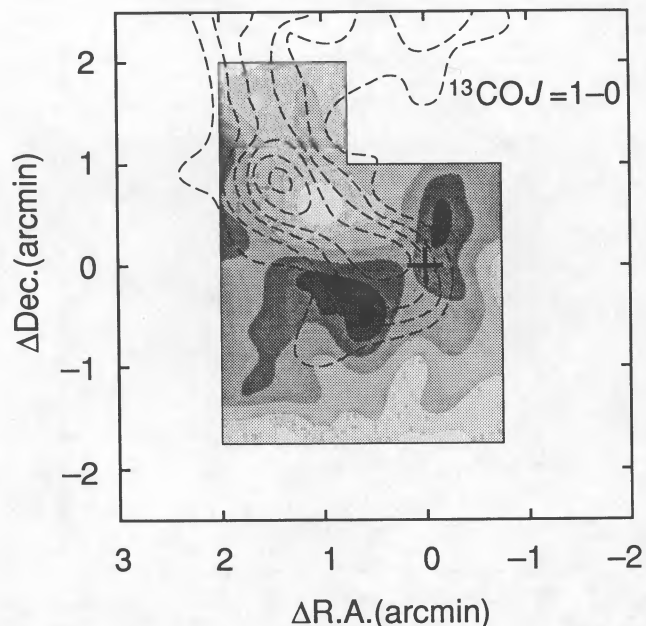


FIG. 7.—Integrated intensity map of ^{13}CO taken with the NRO 45 m telescope (*gray scale*). The map of the CO blue lobe is superposed as a thin dashed line. The integration range for the ^{13}CO map is from -5.4 to -3.0 km s^{-1} . The lowest contour is at 5.6 K km s^{-1} , and the contour step is 0.8 K km s^{-1} . The mapped area with $15''$ grid spacing interval is indicated by a thin-lined box. The cross indicates IRAS 22266+6845.

TABLE 3

PHYSICAL PARAMETERS OF DENSE CORES

Core	Cloud Size ^a	Mean Radius ^b (pc)	Mass ^c (M_{\odot})	Mean Density ^d (cm^{-3})
^{13}CO	9.5×10.5	0.30	30	3.9×10^3
C^{18}O	5.4×6.3	0.17	6	5.0×10^3
CS	2.0×2.2	0.06	-2^e	$\sim 4 \times 10^{4e}$

^a Cloud size is described as the diameters of the major and minor axes at half-intensity level.

^b Mean radius is computed as the geometrical mean of the radius of the major and minor axes.

^c Excitation temperature was assumed to be 12 K.

^d Mean density was computed by assuming that the spherical core with the mean radius includes the derived mass.

^e The mass of the CS core was estimated by assuming a spherical core with mean radius of 0.06 pc and mean density of $\sim 4 \times 10^4$ cm^{-3} (see text).

to have been excluded. In fact, the column density of molecular hydrogen gas toward this ^{13}CO minimum is $N(\text{H}_2) \sim 3.5 \times 10^{21} \text{ cm}^{-2}$, which is $\sim 30\%$ of that toward the ^{13}CO maximum at $(45'' - 30'')$ ($\sim 1.2 \times 10^{22} \text{ cm}^{-2}$) or $\sim 70\%$ of the column density averaged over the observed area ($\sim 5 \times 10^{21} \text{ cm}^{-2}$). Thus, the gas distribution of the parent cloud has a cavity at the CO blue lobe. On the other hand, we cannot state whether there is also a hole or bay structure toward the red lobe, because the ^{13}CO observations do not cover the red lobe. Such anticorrelation between the ^{13}CO distribution and the outflow has been noted only in the cases of L1551 (Moriarty-Schieven & Snell 1988; Hayashi, Hayashi, & Kaifu 1989) and B335 (Hirano et al. 1991). The present case provides another piece of evidence for a cavity in the molecular cloud.

Furthermore, the ^{13}CO distribution shows some enhancements surrounding the blue lobe of the CO outflow. There is a peak on the east side where the CO blue lobe changes its direction from northeast to north. The regions of higher column density delineate the southeastern limb of the blue lobe of the CO outflow. In addition, at the northwest side of the blue lobe, we can recognize the weak ^{13}CO ridge surrounding the blue lobe of the outflow. These enhancements may consist of the swept-up gas due to the outflow.

3.4. Kinematics of the Ambient Gas

In the velocity field of the ambient gas, we find evidence of the acceleration of the ambient gas by the outflow. In Figure 8, we show the position-velocity (p - v) diagram of the ^{13}CO line along the north-south axis at right ascension offset $\Delta\text{R.A.} = +90''$. The hatched area indicates the range over which the CO blue wing is seen. The peak velocity of ^{13}CO toward the CO blue lobe is shifted blueward by $\sim 0.5 \text{ km s}^{-1}$ with respect to that outside the CO blue lobe. This velocity shift can be observed toward most of the CO blue lobe. On the

other hand, the ^{13}CO observations do not cover the CO red lobe.

For the dense gas we also found evidence for acceleration. The p - v diagram of the CS line along the north-south axis at right ascension offset $\Delta\text{R.A.} = +30''$ is shown in Figure 9. The CS emission clearly shows a velocity shift toward the blue lobe of the outflow (indicated by the hatched area). The peak velocity of the CS emission at $\Delta\text{decl.} = 0''$ is shifted blueward by $\sim 0.8 \text{ km s}^{-1}$ with respect to the gas at $\Delta\text{decl.} < -30''$. The velocity-shifted component of the CS emission is seen within the blue lobe of the CO outflow. The velocity shift in CS is larger than that in ^{13}CO . This can be interpreted as the overlap of the undisturbed component of the optically thick ^{13}CO emission with the blueshifted component. It is probable that there is a lot of unperturbed gas along the line of sight because the outflow occupies only a small area in the molecular cloud on the sky plane. On the other hand, the CS emission traces well only the blueshifted component without overlapping the undisturbed component, because the size of the CS core is smaller than that of the outflow.

The HCO^+ line spectrum toward the IRAS source has two velocity components. One component ($T_R^* = 2.3 \text{ K}$) is at the systemic velocity of the HCO^+ core, and other component ($T_R^* = 2.3 \text{ K}$) is shifted blueward by $\sim 1.4 \text{ km s}^{-1}$. The blueshifted component is seen only near the IRAS source. The HCN line also shows the blueshifted component ($T_R^* = 1.0 \text{ K}$) toward the IRAS source, where we obtained a spectrum with a higher signal-to-noise ratio (the rms noise level is $\sim 0.15 \text{ K}$).

4. DISCUSSION

4.1. Dynamical Interaction of the Outflow with the Ambient Cloud

Molecular outflows have enormous mechanical energies and momenta, so they have a significant influence on the ambient

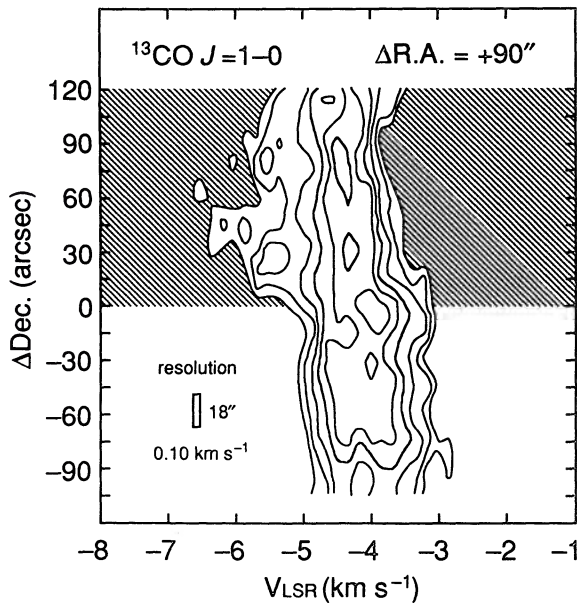


FIG. 8.—Position-velocity diagram of the ^{13}CO line along the north-south axis at right ascension offset $\Delta\text{R.A.} = +90''$ from the IRAS point source. The hatched area indicates a spatial range over which the blue wing of the CO outflow is seen. Contours are from 1.6 K with 0.8 K step. The tick on the ordinate denote the observed points.

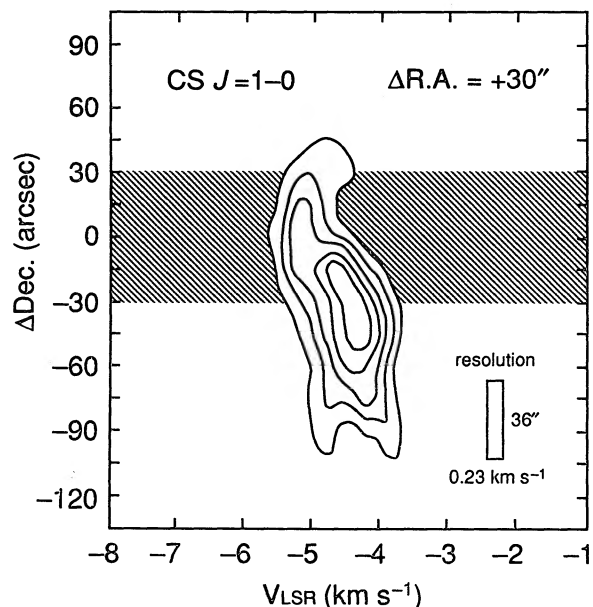


FIG. 9.—Same as Fig. 8, but for the CS line at right ascension offset $\Delta\text{R.A.} = +30''$. Contours are from 0.6 K with 0.3 K step. The tick marks denote the observed points.

material. In the previous section, we have shown that the intensity of the quiescent molecular cloud gas is depressed at the blue lobe of the CO outflow. In addition, there is some blueshifted gas at the blue lobe of the CO outflow. These results strongly suggest that the molecular outflow in L1221 dynamically interacts with its ambient material.

In order to certify this possibility, we compare the momentum and energy of the velocity-shifted gas with those of the blue lobe of the outflow. The mass of the blueshifted ambient gas probed by the ^{13}CO emission is estimated to be $\sim 1.0 M_{\odot}$ within the mapped area, as shown in Figure 7. However, this might be a lower limit because our ^{13}CO map covers only half the area of the CO outflow. If the gas also shows the blueshifted velocity throughout the blue lobe of the CO outflow, the mass of the blueshifted component should be multiplied by a factor of 2. Assuming that all the material of the above mass is moving at the velocity of $\sim 0.5 \text{ km s}^{-1}$ as observed in ^{13}CO , we obtain the momentum and kinematic energy of disturbed gas to be $0.5\text{--}1.0 M_{\odot} \text{ km s}^{-1}$ and $(3\text{--}5) \times 10^{42}$ ergs, respectively. These values are smaller than those of the blue lobe of the CO outflow determined from the radial component of the observed velocity, and they are $\sim 30\%\text{--}50\%$ in momentum and $\sim 10\%\text{--}20\%$ in energy of the blue lobe, respectively. If we take the shift velocity to be $\sim 0.8 \text{ km s}^{-1}$ as observed in CS, the momentum and energy of the shifted gas are $\sim 50\%\text{--}100\%$ and $\sim 20\%\text{--}50\%$ of the CO blue lobe, respectively. The outflow has momentum and energy enough to explain the observed velocity shift. Therefore, we suggest that this acceleration of the ambient gas has been caused by dynamical interaction of the outflow, and that the surrounding material has been substantially disrupted and moved out. In some cases, the acceleration of the ambient gas due to dynamical interaction of outflows has been noted (e.g., NGC 2071 North: Iwata, Fukui, & Ogawa 1988; L1251: Sato & Fukui 1989; ρ Oph East: Mizuno et al. 1990). The present observations provide a clearer example showing that the molecular outflow has dynamically affected the surrounding gas. The outflow will not only alter the ambient cloud structure but will also remove the material surrounding the star on a small scale. The *IRAS* source does not coincide with the peak of the dense core. It is known that infrared sources are not always found at the emission peaks of the dense cores (e.g., Beichman et al. 1986; Clark 1987), and such cases might be explained in terms of the destruction of the dense core by the outflow (e.g., Myers et al. 1988; Mathieu et al. 1988). The blueshifted HCO^+ and HCN emissions localized at the *IRAS* source may represent the matter being stripped by the outflow from the vicinity of a star. *IRAS* 22266+6845 has a warm far-infrared spectrum $\{\log [F_{\nu}(12)/F_{\nu}(25)] = -0.50$ and $\log [F_{\nu}(25)/F_{\nu}(60)] = -0.53\}$, which is similar to those of T Tauri stars (Harris 1985; Beichman et al. 1986); we suggest that this source is at a late stage of protostellar evolution. The outflow will ultimately reveal a newly formed star embedded in the cloud.

4.2. U-shaped Structure of the Outflow

The outflow studied here show a remarkably bent U-shaped structure open to the northwest. In most of the outflow objects, blue- and redshifted emission is symmetrically displaced with respect to the driving source. Such a U-shaped morphology is seen in some extragalactic radio jets such as NGC 1265, which is understood to result from the motion of a galaxy through an intercluster medium (e.g., Miley, Wellington, & van de Laan

1975; Owen, Burns, & Rudnick 1978). What has caused such an U-shaped structure of the molecular outflow? The proper motion of the driving source with respect to the ambient molecular cloud would not be responsible for the U-shaped morphology, because the required velocity ($\sim 7 \text{ km s}^{-1}$) is considerably larger than the velocity dispersion of T Tauri stars relative to the associated molecular cloud gas which is 1.5 km s^{-1} or less (Hartman et al. 1986). We present two possibilities to explain the U-shaped morphology: (1) the influence of an external pressure and (2) guiding by bent magnetic fields.

In § 3.3 we investigated the distribution of the cloud material around the outflow in L1221, and we found that dense gas exists on the southeast and east sides of the CO blue lobe. This appearance suggests that the outflow has gradually changed its direction through interaction with the ambient dense material. It appears that the dense material regulates the direction of the outflow. However, this is likely to be impossible, for the following reason. The mass of the dense gas material where the blue lobe changes its direction to the north from the northeast is estimated to be $\sim 0.3 M_{\odot}$, assuming a sphere with a radius of 0.03 pc and a density of $4 \times 10^4 \text{ cm}^{-3}$. If this material dams up the outflow, it will undergo the force of the outflow, which is $3.6 M_{\odot} \text{ km s}^{-1}$ (geometrical average momentum of case I and case II for the blue lobe)/ $5 \times 10^4 \text{ yr}$. By this force, the material will be accelerated at the velocity of 12 km s^{-1} and blown off to a distance 0.3 pc from the driving source during the outflow event. This is inconsistent with the present observational results. This indicates that an external agency to restrain the dense material and the outflow is required.

L1221 has a cometary appearance characterized by the dense head with a sharp boundary in a certain direction and the extended tail in the opposite direction, and the symmetry axis of the U-shaped outflow is aligned with this cloud elongation. Such a configuration reminds us that these are caused by an external pressure. A similar example of the influence of an external pressure is observed in a bright-rimmed globule in the old H II region IC 1396 (Sugitani et al. 1989). To explain the U-shaped outflow in L1221, the external pressure must be comparable to the dynamical gas pressure of the outflow, $P_{\text{flow}} \sim E_{\text{flow}}/V_{\text{flow}}$. Here E_{flow} and V_{flow} are the kinematic energy and volume of the outflow, respectively. Assuming that the pathlength of the outflow along the line of sight is 0.12 pc , we obtain $P_{\text{flow}}/k \sim 4 \times 10^6 \text{ cm}^{-3} \text{ K}$. This value is, for example, close to the pressure of typical H II regions, $6 \times 10^6 \text{ cm}^{-3} \text{ K}$ (Myers 1978). The appearance of L1221 can be consistently explained if there are external pressure sources, but we have not observationally established yet that H II regions or stellar winds actually interact with the L1221 globule. On the other hand, one may think that L1221 is moving in the rest ambient material. However, such a scenario requires an extremely large velocity for L1221. Because we did not detect CO emission outside L1221, the density of the ambient material must be smaller than 10^2 cm^{-3} .

Thus, in order to obtain the pressure above, the velocity of L1221 relative to the ambient material should be greater than 25 km s^{-1} , but this velocity is too large compared with the velocity dispersion of interstellar clouds (e.g., Magnani, Blitz, & Mundy 1985). We consider that external pressure from old H II regions or stellar winds is a plausible explanation accounting for both the U-shaped morphology of the outflow and the cometary shape of the globule, although we have no observational support as yet.

Another probable explanation of the U-shaped morphology

is that the shape of the outflow has been affected by bent ambient magnetic fields. Recent polarimetric studies have shown that the direction of the well-collimated, bipolar molecular outflow tends to be aligned with ambient magnetic fields (e.g., Sato et al. 1985; Vrba et al. 1986; Strom et al. 1986). Theorists have suggested that the magnetic field must play an important role in the acceleration and collimation of the outflow (e.g., Pudritz & Norman 1983, 1986; Uchida & Shibata 1985; Shibata & Uchida 1986). From the near-infrared polarimetry of background stars, Hodapp (1987) has revealed that magnetic fields in star-forming cometary globules are clearly bent; the magnetic field in the cloud head is perpendicular to the tail, where the magnetic field is parallel to its elongation. Such bent magnetic fields would have been formed in the course of the formation of the cometary cloud by an external agency (Hodapp 1987). If magnetic fields in L1221 showed a bent U-shaped structure, the outflow would be guided by bent magnetic fields. In order to test the above interpretation, we have to investigate the magnetic field configuration in this region. Optical polarization measurements of stars in this region have been carried out by M. Seki (1989, private communication). The obtained magnetic field distribution is a little complicated, so we cannot establish whether there is a bent magnetic field or not. However, there is a possibility that several stars are foreground stars, not related to the cloud. There remains a possibility that magnetic fields play an important role in determining the outflow morphology, and we need more polarization and excitation measurements of stars in the direction of the L1221 cloud.

5. CONCLUSIONS

We summarize the main conclusions of the present study as follows:

1. We have discovered a bipolar CO outflow associated with

IRAS 22266 + 6845 in the cometary dark cloud L1221. This outflow shows an unusual bent U-shaped structure.

2. The spatial distribution of the ^{13}CO intensity shows an anticorrelation with the blue lobe of the CO outflow, and the ambient gas is thought to be excluded by the outflow. There is a dense gas ridge probed by CS and C^{18}O , which delineates the eastern limb of the blue lobe. The blue lobe of the outflow changes its direction in accordance with this ridge.

3. We have obtained clear evidence for dynamical interaction of the outflow with the ambient material. The ambient ^{13}CO and CS molecular gas shows a blueward velocity shift at the blue lobe of the outflow. The outflow has momentum large enough to cause this velocity shift.

4. Some kind of external pressure, which has also formed the cometary shape of the globule, may play an important role in forming the remarkable U-shaped morphology of the CO outflow and the dense gas ridge delineating this outflow.

It is our pleasure to acknowledge many useful comments by Professors K. Kawabata and T. Nakano. We would like to thank the staff of NRO for help in observations and in data reduction. Thanks are also due to H. Ogawa for his critical comments and his excellent work on the development of the receiver system of the 4 m radio telescope. We also thank Professor M. Seki for communicating information on the polarimetry of this region and for useful suggestions. We wish to acknowledge valuable discussions with K. Tatematu, S. Yamamoto, A. Mizuno, T. Iwata, M. Nakayama, and N. Ohashi. We thank Miss T. Tosaki for assistance during the observations at Nobeyama. This research was in part financially supported by Grants-in-Aid from the Ministry of Education, Science, and Culture of Japan (Nos. 62420002, 62302008, 63790139, 01790179, 01065002).

REFERENCES

- Beichman, C. A., Myers, P. C., Emerson, J. P., Harris, S., Mathieu, R., Benson, P. J., & Jennings, R. E. 1986, *ApJ*, 307, 337
- Clark, F. O. 1987, *A&A*, 180, L1
- Dickman, R. L. 1978, *ApJ*, 37, 407
- Fukui, Y. 1989, in *Proc. ESO Workshop on Low Mass Star Formation and Pre-Main Sequence Objects*, ed. B. Reipurth (Garching: ESO), 95
- Fukui, Y., Sugitani, K., Takaba, T., Mizuno, A., Ogawa, H., & Kawabata, K. 1986, *ApJ*, 311, L85
- Goldsmith, P. F., Langer, W. D., & Wilson, R. W. 1986, *ApJ*, 303, L11
- Goldsmith, P. F., Snell, R. L., Hemeon-Heyer, M. A., & Langer, W. D. 1984, *ApJ*, 286, 599
- Haikala, L. K., & Dietrich, O. 1989, in *Physics and Chemistry of Interstellar Molecular Clouds: Millimeter and Submillimeter Observations in Astrophysics*, ed. G. Winnewisser & J. T. Armstrong (Berlin: Springer-Verlag), 236
- Harris, S. 1985, in *Proc. ESO-IRAM-Onsala Workshop on (Sub)millimeter Astronomy*, ed. P. A. Shaver & K. Kjar (Garching: ESO), 527
- Hartman, L., Hewett, R., Stahler, S., & Mathieu, R. D. 1986, *ApJ*, 309, 275
- Hayashi, S. S., Hayashi, M., & Kaifu, N. 1989, in *Structure and Dynamics of the Interstellar Medium*, ed. G. Tenorio-Tagle, M. Moles, & J. Melnick (Berlin: Springer-Verlag), 260
- Heyer, M. H., Snell, R. L., Goldsmith, P. F., & Myers, P. C. 1987, *ApJ*, 321, 370
- Hirano, N., Kameya, O., Nakayama, M., & Takakubo, K. 1988, *ApJ*, 327, L69
- Hirano, N., Kameya, O., Umemoto, T., Kuno, N., & Takakubo, K. 1991, in preparation
- Hodapp, K.-W. 1987, *ApJ*, 319, 842
- IRAS Point Source Catalog. 1988, Joint IRAS Science Working Group (Washington, DC: GPO)
- Iwata, T., Fukui, Y., & Ogawa, H. 1988, *ApJ*, 325, 372
- Kaifu, N., et al. 1984, *A&A*, 134, 7
- Kawabata, K., Ogawa, H., Fukui, T., Takano, T., Fujimoto, Y., Kawabe, R., Sugitani, K., & Takaba, H. 1985, *A&A*, 151, 1
- Kutner, M. L., & Ulich, B. L. 1981, *ApJ*, 250, 341
- Lada, C. J. 1985, *ARA&A*, 23, 267
- Levrault, R. M. 1988, *ApJ*, 330, 897
- Lynds, B. T. 1962, *ApJS*, 7, 1
- Magnani, L., Blitz, L., & Mundy, L. 1985, *ApJ*, 295, 402
- Margulis, M., & Lada, C. J. 1986, *ApJ*, 309, L87
- Margulis, M., Lada, C. J., & Snell, R. L. 1988, *ApJ*, 333, 316
- Mathieu, R. D., Benson, P. J., Fuller, G. A., Myers, P. C., & Schild, R. E. 1988, *ApJ*, 330, 385
- Miley, G. K., Wellington, K. J., & van der Laan, H. 1975, *A&A*, 38, 381
- Mizuno, A., Fukui, Y., Iwata, T., & Takano, T. 1990, *ApJ*, 356, 184
- Moriarty-Schieven, G. H., & Snell, R. L. 1988, *ApJ*, 332, 364
- Myers, P. C. 1978, *ApJ*, 225, 380
- Myers, P. C., Heyer, M., Snell, R. L., & Goldsmith, P. F. 1988, *ApJ*, 324, 907
- Neckel, Th., & Vehrenberg, H. 1987, *Atlas of Galactic Nebulae*, Vol. 2 (Düsseldorf: Treugesell)
- Owen, F. N., Burns, J. O., & Rudnick, L. 1978, *ApJ*, 226, L119
- Pudritz, R. E., & Norman, C. A. 1983, *ApJ*, 274, 677
- . 1986, *ApJ*, 301, 571
- Sato, F., & Fukui, Y. 1989, *ApJ*, 343, 778
- Sato, S., Nagata, T., Nakajima, T., Nishida, M., Tanaka, M., & Yamashita, T. 1985, *ApJ*, 291, 708
- Shibata, K., & Uchida, Y. 1986, *PASJ*, 38, 631
- Snell, R. L. 1981, *ApJS*, 45, 121
- Snell, R. L., Langer, W. D., & Frerking, M. A. 1982, *ApJ*, 255, 149
- Snell, R. L., & Schloerb, F. P. 1985, *ApJ*, 295, 490
- Strom, K. M., Strom, S. E., Wolff, S. C., Morgan, J., & Wenz, M. 1986, *ApJS*, 62, 39
- Sugitani, K., Fukui, Y., Mizuno, A., & Ohashi, N. 1989, *ApJ*, 342, L87
- Uchida, Y., & Shibata, K. 1985, *PASJ*, 37, 515
- Vrba, F. J., Luginbuhl, C. B., Strom, S. E., Strom, K. M., & Heyer, M. H. 1986, *AJ*, 92, 633